JOURNAL OF AIRCRAFT
Vol. 33, No. 4, July–August 1996

Hodograph Method for Airfoil Design: The General Case

Alejandro C. Limache*
Universidad Nacional de Córdoba, Córdoba 5000, Argentina

Many airfoils, including all of the symmetric airfoils, generate flows such that the velocity–contour (i.e., the contour defined on the hodograph plane by the vector velocities of the airfoil's boundary) self-intersects. This self-intersection implies that in different points of the space the flow has the same vector velocity. In such cases the classical hodograph theory fails and it is impossible to use the velocity–contours for designing such airfoils. A mathematical extension of the theory is developed to remedy the failure. This extended theory is then successfully applied to develop a general inverse method for designing airfoils that generate all of the dynamic and geometric requirements imposed in the input velocity–contour. It is also shown that there exists not only one, but an infinite number, of airfoils capable of generating exactly the same input self-intersecting velocity–contour.

Nomenclature

C_L = lift coefficient
C_p = pressure coefficient
$C_{\xi 0}$ = auxiliary non-self-intersecting closed contour
$F(Z)$ = function that defines the velocities of a flow in a region R_Z
n = coordinate perpendicular to the flow direction
p = pressure
$\boldsymbol{q}$, q = vector velocity and speed of the flow, respectively
q_0, α = speed and angle of the freestream incident on the circular obstacle in the z plane
q_∞ = design speed of the freestream incident on the designed airfoil
R = radius of the circular obstacle in the z plane
R_V = region in the V plane that contains all of the complex velocity values taken
R_Z = region of the physical plane defined by all of the points around the airfoil
R_z = region of the z plane exterior to the circular obstacle
$R_{\xi 0}$ = region defined by the contour $C_{\xi 0}$
S = forward stagnation point on the airfoil
s = coordinate tangent to the airfoil surface
T = trailing edge of the airfoil
u, v = X and Y component of the velocity, respectively
V = complex velocity, $u - iv = qe^{i\theta}$
V_∞ = complex velocity of the freestream, $q_\infty e^{-i\theta_\infty}$
w_S, w_T = points in the w plane that correspond to points S and T on the airfoil, respectively, e.g., V_T is the point in the V plane (hodograph) that defines the velocity of T
Z = complex variable whose components X, Y define the coordinates of a two-dimensional physical plane
z = complex variable whose components x, y define a two-dimensional plane with a circular obstacle centered at the origin
Γ = circulation
θ = direction of the velocity
θ_∞ = design incidence of the freestream incident on the designed airfoil
ξ, ξ_0, w = auxiliary complex variables
ρ = density, ρ_S = density of the stagnation point S
ϕ = angular coordinate around the circular obstacle in the z plane
ψ, φ, W = the stream function, velocity potential, and complex potential $\varphi + i\psi$ of the flow, respectively

Received June 3, 1995; revision received Dec. 27, 1995; accepted for publication Jan. 15, 1996.

*Researcher, SeCyT, FaMAF, Department of Aeronautics (FCEFyN).

Introduction

IN the usual problem of direct analysis the position coordinates (X, Y) or contour defining an airfoil are given, and then the dynamics, i.e., the resulting velocities $(u, v) = F(X, Y)$ on the airfoil, are determined by solving the flow equations. Conversely, an inverse method is set up by giving the desired dynamics, i.e., some kind of information about the velocities $(u, v) = (q \cos \theta, q \sin \theta)$ of the flow corresponding to the airfoil's boundary, and the problem consists of finding the coordinates (X, Y) defining the airfoil that generate such dynamics. Simplifying, an inverse method consists of finding F^{-1} such that $F^{-1}(u, v) = (X, Y)$.

Different exact inverse methods for airfoil design have been devised in the last few decades. The first inverse method that deserves to be mentioned is the method of Lighthill[1]; his incompressible method determines exactly the shape of the airfoil in terms of the velocity distribution $q = q(\phi)$ of the airfoil prescribed as a function of ϕ, the angular coordinate around the circle in an auxiliary z plane into which the airfoil may be transformed. The harmonic conjugate θ of q, that is, the direction of the velocity, is found as a function of ϕ by means of Poisson's integral or by an appropriate series development of the complex velocity $V = qe^{-i\theta}$. Since the flow around the circle is known, the airfoil can be found by integration of the equation

$$Z = \int \frac{1}{V} \frac{dW}{dz}\, dz \tag{1}$$

for $z = Re^{i\phi}$. The method of James, used by Liebeck[2] to design his airfoils, improved the method of Lighthill[1] because the velocity distribution $q = q(s)$ is given in terms of the arc length s along the unknown airfoil's surface. This gives more direct control over the pressure gradients.

Woods[3] uses an auxiliary z plane that contains a given geometry different from the circular obstacle (usually a infinite strip). Then, using a generalized Poisson's integral he finds V in terms of z given mixed boundary conditions: he prescribes q over a portion of the boundary and the geometry (i.e., θ) on the rest. The map from the complex potential W plane ($W = \varphi + i\psi$) to the z plane is known, and then he can integrate

Eq. (1) to find the airfoil. The method applies only to the design of symmetric airfoils because information about q or θ is required along all of the streamline that impact on the airfoil.

Recently, Volpe[4] has developed a physical-stretching-based inverse method to design airfoils at transonic conditions. Again, the airfoil is obtained by prescribing the velocity distribution $q(s)$. He proceeds as follows: first, he determines how the compressible flow equations and the components (u, v) of the velocity transform by a stretching of the physical plane Z, i.e., by a conformal mapping. Then, he prescribes q (i.e., the tangential component of the velocity) along the s of a known airfoil and transforms the region exterior to this airfoil to the interior of a circular disc; this gives q in terms of ϕ and sets up the appropriate boundary conditions for the physical-stretched flow equations. Once these equations are solved a nonzero normal component of velocity is obtained along the boundary of the known airfoil. This is not surprising since the known airfoil is not the correct geometry that generates the distribution $q = q(s)$. Finally, this normal component velocity distribution is used to generate a new geometry, and the process restarts iteratively.

Jameson[5] has developed an inverse method for compressible flow using similar concepts as the ones used by Volpe,[4] but now he regards the design problem as a control problem in which the control is the shape of the airfoil's boundary and the desired objective is measured by a cost function I [this may, for example, measure the deviation from a desired pressure $p = p(s)$ or velocity distribution $q = q(s)$], then the solution is found by minimizing I subject to the constraints defined by the flow equations.

Drela and Giles[6] have developed a new technique of analysis for transonic flows around single airfoils. The technique has also been applied as a compressible mixed-inverse method. In this sense the geometry of all the airfoil is given, except in the upper surface where the required pressure distribution is given, then the method completes the geometry of the airfoil in such a way to generate the input pressure distribution. The method has the advantage that the problem is solved directly on the physical plane and that the flow equations are solved in a conservative way.

The semi-inverse compressible method of Bauer et al.[7] should also be mentioned. It is based on proposing an appropriately parametrized candidate solution, obtained from a generalization of an explicit solution obtained in the incompressible case for a particular family of symmetric airfoils. The candidate solution has unknown functions that are determined by solving the linear equations that result from inserting the candidate solution in the transformed potential flow equations defined in a plane of complex characteristics. The airfoil is obtained by prescribing in the plane of complex characteristics some points that will probably correspond to the streamline $\psi = 0$, which is the streamline that defines the airfoil. The method is not very practical and it is hard to work automatically.

Other inverse methods are the ones based on the hodograph method, and they differ from the nonhodograph methods[1-6]: both q and θ corresponding to each point of the airfoil's surface are given simultaneously as input information, this cannot be done in the nonhodograph methods, since if the two values are given, the boundary conditions are not well-posed. Hodograph methods have the advantage that dynamic and geometric information can be prescribed simultaneously on each point of the surface of the unknown airfoil. The input values (q, θ) are not prescribed in terms of s (this is the cost hodograph methods pay), they are simply put on the V plane (hodograph). These prescribed values define a contour called velocity–contour (VC). In this sense, a VC is a contour on the hodograph that defines the successive values of velocity $\boldsymbol{q} = (u, v)$ of the flow as it goes around the airfoil surface. In Fig. 1, one can see the VC of a Joukowski airfoil for an incidence of 0.5 deg of the uniform stream. The points $V_S = 0 + i0$ and V_T correspond

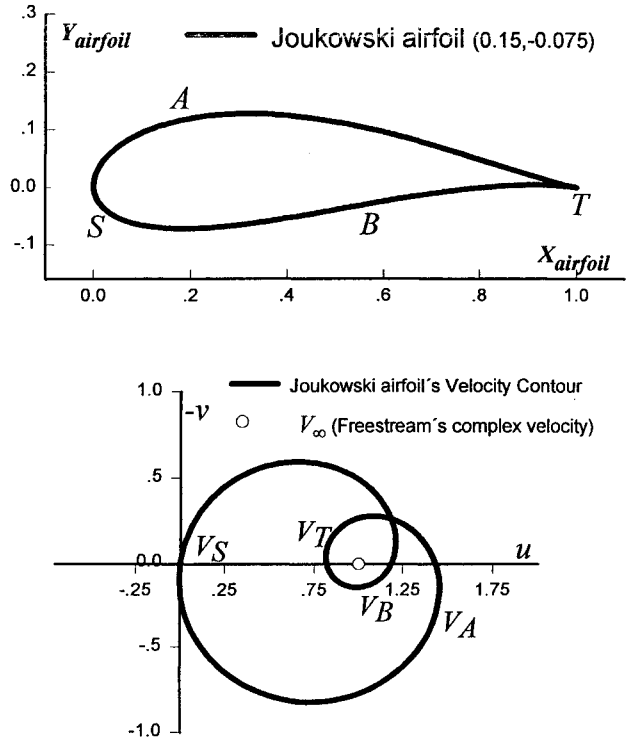

Fig. 1 Relation between a Joukowski airfoil and its velocity–contour corresponding to a freestream incidence of 0.5 deg.

to the complex velocities of the flow at the point of impact S and at the trailing edge T of the airfoil, respectively. The points V_A and V_B are the complex velocities of the points A and B on the airfoil surface, whereas the point V_∞ is the complex velocity of the uniform stream incident on the airfoil, i.e., $V_\infty = 1 \exp\{-i[0.5(\pi/180)]\}$.

Two inverse hodograph methods for airfoil design have recently appeared in the literature. One is the hodograph method of Cohen.[8] He developed a method for designing a family of rooftop airfoils. The method uses as input a particular family of VCs, which in the $\ell n\ V$ plane can be represented as polygons, each line being parallel to one of the coordinate axes. The well-known Schwarz–Christoffel transformation can be used to map the polygonal regions onto the upper half-plane of the z plane. This gives V in terms of z, then Eq. (1) is used to find the airfoils.

More recently, Limache[9] devised a hodograph method that easily obtains the shape of the airfoils that generate exactly the dynamic and the geometric behavior imposed by arbitrary non-self-intersecting velocity–contours on the hodograph. A non-self-intersecting contour is any closed contour that does not cross itself. An example of a non-self-intersecting VC is given in Fig. 2. Figure 1 shows a typical self-intersecting VC. Briefly, this method can be described as follows: the auxiliary z plane is chosen to be the plane that contains a circular obstacle of radius R in the origin. Since the flow around a circular obstacle is known, dW/dz is known exactly once V is expressed in terms of z. It turns out that the key problem is to find the appropriate conformal mapping that maps the non-self-intersecting contour on the hodograph into the circle in the z plane. Once this is solved, the speed q_∞ and the incidence θ_∞ of the freestream incident on the airfoil, under which the input requirements and the physical constraints are satisfied, can be found by solving a single complex equation. Finally, the shape of the airfoil is determined by the integration of Eq. (1). In particular, the method is able to generate all of the airfoils of Cohen's method[8] because the VCs proposed by Cohen are non-self-intersecting. The method is very general, except that it fails in that it is not able to work with self-intersecting velocity–contours.

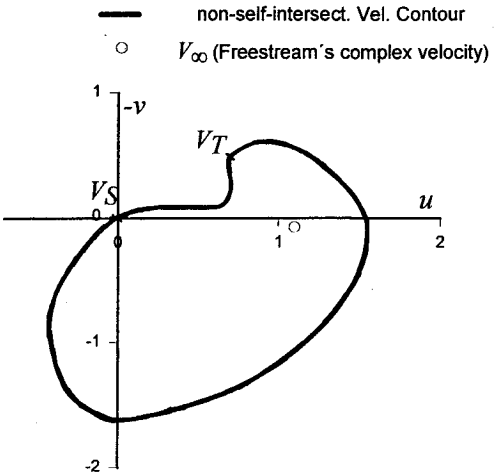

Fig. 2 Example of a non-self-intersecting velocity–contour.

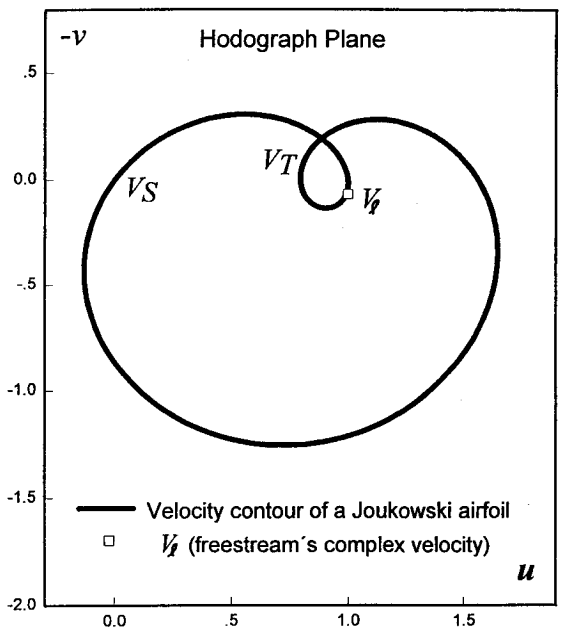

Fig. 3 Self-intersecting velocity–contour of a Joukowski airfoil.

It can be seen that there exist airfoils (including many known airfoils) that generate flows, such that, the velocity–contour self-intersects. For example, the Joukowski airfoils generate this kind of VC (as shown in Fig. 1 or 3 for different freestream incidences). It also can be seen that all of the symmetric airfoils generate self-intersecting VCs (inclusively at a nonzero incidence), as can be viewed in Fig. 4 for the particular case of the NACA 0012 airfoil. From this, one deduces that a large class of airfoils (which may have a good behavior) cannot be designed by the method of Ref. 9. The problem is serious because it turns out that in the cases of self-intersecting VCs, not only the method presented in Ref. 9 fails, but the hodograph method fails in general. Herein, lies one of the objectives of this article: to show how all of these lost solutions can be recovered by an extension of the classical hodograph theory. First, it will be helpful to look at the types of velocity–contours and the topology that they generate.

Types of VCs, Mathematical, and Physical Properties

Consider a region R_Z, with boundary defined by an obstacle or airfoil, of a two-dimensional Z plane. The motion of a flow uniform at infinity in the region R_Z is described by some function $F(Z) = V = u - iv$. Since F is continuous, the image by

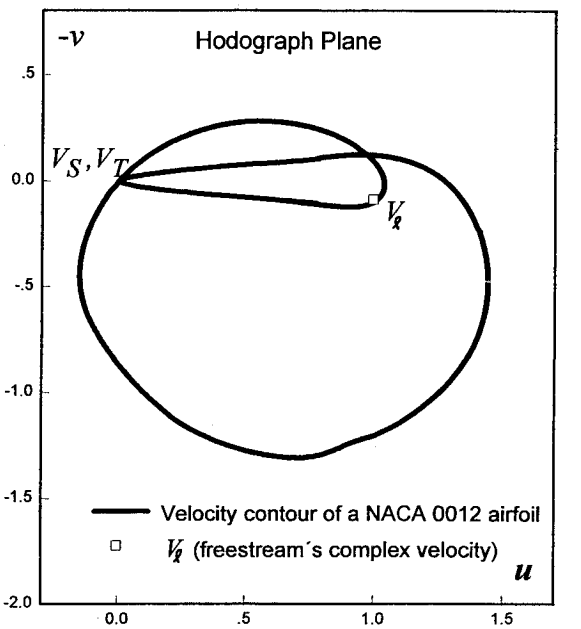

Fig. 4 Self-intersecting velocity–contour of the NACA 0012 airfoil.

F of the points of the region R_Z is a well-defined region R_V at the hodograph plane, which defines all of the velocity values V attained by the flow. If a value of V is taken by the flow in more than one point Z, one says that R_V is an overlapping region. The image by F of the boundary of R_Z is by definition the velocity–contour. It turns out by continuity that, given the VC it uniquely defines the shape of the region R_V, however, the converse is not true because the boundary of R_V is not necessarily equal to the VC.

If the VC is a simple (non-self-intersecting) contour as the one shown in Fig. 2, then the region R_V is the region inside the VC and is a simple (without holes and nonoverlapping) region. Obviously, the boundary of R_V coincides with the VC. From this one can deduce that there is a one-to-one correspondence between each point Z of R_Z and each point V of R_V, and that the function F is one-to-one.

If the VC self-intersects then, remembering the definition of the VC, there are two points Z_{np1} and Z_{np2} on the airfoil's surface that have exactly the same vector velocity. Furthermore, it turns out that on R_Z there exist two subregions R_{Z1} and R_{Z2}, one containing the point Z_{np1} and the other containing the point Z_{np2}, such that their image by the function F satisfies

$$F(R_{Z1}) = \text{zone of overlapping} = F(R_{Z2}) \tag{2}$$

This proves that in this case F is many-to-one and that the region R_V overlaps.

Any given self-intersecting VC is at most a combination of the following two cases:

Case 1: The velocity–contour has a single point of self-intersection and has a remaining part that goes into the region R_V, forming a loop (or loops) that determines the zone of overlapping R_V. R_V continues being a region without holes. In Fig. 5a this kind of VC is shown, the zone of overlapping corresponds to the shadowed zone.

Case 2: The velocity–contour self-intersects in two points, forming a region R_V that has the shape of a deformed annulus, i.e., R_V is a region with a hole inside. Figure 5b shows that this kind of VC may appear when one wants to design a high-lift airfoil with finite trailing-edge angle. The zone of overlapping of this kind of VC is shown as the shadowed region in Fig. 5b.

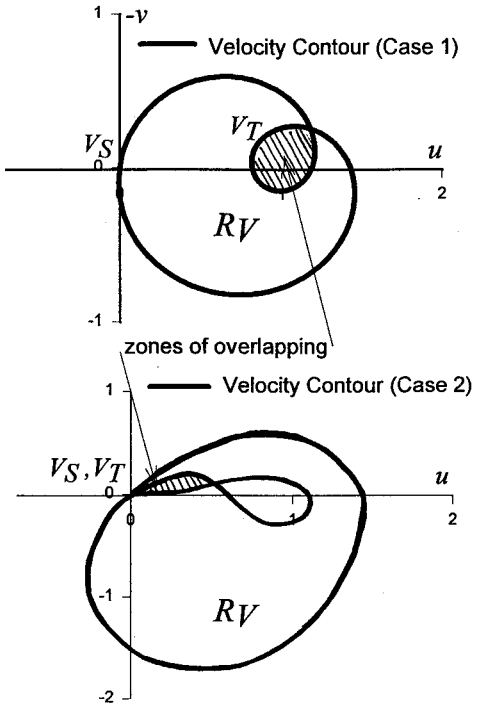

Fig. 5 Types of self-intersecting velocity–contours and their corresponding region R_V.

The character of the boundary conditions is such that in the nonhodograph methods the physical planes or one equivalent stretched plane play the principal roll, inclusively the hodograph plane does not need to be mentioned. On the contrary, in the hodograph methods the hodograph, and in particular the topology of the region R_V defined by the VC, are of great importance. For example, the Cohen's method[8] works only with polygonal regions $R_{\epsilon nV}$, and the method of Ref. 9 is restricted by the condition that the regions R_V do not overlap. In the next section the failure of the hodograph methods for self-intersecting VCs (i.e., for overlapping R_V) is further discussed.

Compressible Hodograph Technique and the Problem of an Overlapping R_V

The compressible hodograph method is an old technique that was developed, when computers were not available, to solve direct problems. The book of von Mises[10] contains a complete description of this technique and it will be followed in the first part of the discussion of this section. The underlying idea was to develop a technique to transform the difficult problem of solving a nonlinear partial differential equation (PDE) into the easier one of solving a linear PDE. This was achieved by switching the role of the independent coordinates from the (X, Y) position coordinates to the velocity coordinates (q, θ) or (u, v). This switch or change of variables modifies the nonlinear differential equations for irrotational flow in such a way that second-order linear equations for φ and ψ with the velocity coordinates as the independent variables are obtained. For example, the linear equation for ψ with (q, θ) as velocity coordinates yields Chaplygins's equation:

$$\frac{\partial^2\psi}{\partial q^2} + \frac{1 - M^2}{q^2}\frac{\partial^2\psi}{\partial\theta^2} + \frac{1 + M^2}{q}\frac{\partial\psi}{\partial q} = 0 \tag{3}$$

Hence, if one finds $\psi(q, \theta)$ in some region R_V of the hodograph plane, the relation between the coordinates (X, Y) in the physical plane and the velocity coordinates (q, θ) can be determined by integration:

$$Z = \int \frac{e^{i\theta}\rho_S}{\rho}\left[\left(\frac{\partial\psi}{\partial q} + \frac{i}{q}\frac{\partial\psi}{\partial\theta}\right)d\theta + \left(\frac{M^2 - 1}{q^2}\frac{\partial\psi}{\partial\theta} + \frac{i}{q}\frac{\partial\psi}{\partial q}\right)dq\right] \tag{4}$$

and the problem can be solved. Equation (4) is the generalization of Eq. (1) (which is the limit case $M \to 0$), this is clear as one rewrites Eq. (1) as

$$\begin{aligned} Z &= \int \frac{1}{V}\frac{dW}{dz}\frac{dz}{dV}\,dV = \int \frac{1}{V}\frac{dW}{dV}\,dV \\ &= \int \frac{1}{qe^{-i\theta}}\left(-\frac{\partial\psi}{\partial v} + i\frac{\partial\psi}{\partial u}\right)d(qe^{-i\theta}) \\ &= \int \frac{1}{qe^{-i\theta}}\left[e^{i\theta}\left(-\frac{1}{q}\frac{\partial\psi}{\partial\theta} + i\frac{\partial\psi}{\partial q}\right)\right]e^{-i\theta}\,dq \\ &\quad + \int \frac{1}{qe^{-i\theta}}\left[e^{i\theta}\left(-\frac{1}{q}\frac{\partial\psi}{\theta} + i\frac{\partial\psi}{\partial q}\right)\right](-iq)e^{-i\theta}\,d\theta \end{aligned} \tag{5}$$

Since for a direct problem the boundary conditions are given in the physical plane (e.g., $\psi = 0$ on the boundary of R_Z), the region R_V where Eq. (3) is supposed to be solved cannot be defined. This implies that except for trivial cases the hodograph method is useless for solving direct problems. However, if the switch of variables mentioned previously does not fail, the hodograph provides an excellent tool to solve a well-posed inverse problem (related to a physical situation).

It can be seen that the hodograph theory fails if there exists a point o a line where the Jacobian J of the hodograph–physical plane transformation

$$\begin{aligned} J &= \frac{\partial(u, v)}{\partial(X, Y)} = \frac{\partial(u, v)}{\partial(q, \theta)}\frac{\partial(q, \theta)}{\partial(n, s)}\frac{\partial(n, s)}{\partial(X, Y)} \\ &= -\left[\left(\frac{\partial q}{\partial n}\right)^2 + (1 - M^2)\left(\frac{\partial q}{\partial s}\right)^2\right] \end{aligned} \tag{6}$$

or the Jacobian $j = 1/J$ of the inverse transformation vanishes. It can be demonstrated that, for subsonic flows, J and j can only vanish at isolated points. On the contrary, if $M \geq 1$, it can happen that the Jacobians vanish along lines.

The vanishing of j in a point of the flow region R_Z implies the existence of nonphysical flows. However, the same is not true if J vanishes. The vanishing of J is related to the possibility that there are different points of the flow region R_Z, which have the same vector velocity. In this case, the region R_V overlaps, Eq. (3) cannot be set up, and it is impossible to solve the inverse problem. The root of the problems is clear: the inverse methods have to find the inverse F^{-1} of a function $V = F(Z)$, then, if F is not a one-to-one function, F is not invertible, and the inverse problem cannot be solved.

The problem of finding solutions with the hodograph when R_V overlaps has been solved only for particular cases of exceptional symmetry. The idea is simply to divide the region R_Z into subregions such that one is sure that each subregion generates a subregion of R_V that does not overlap. In airfoil design this only can be done for the case of designing symmetric airfoils at zero incidence, i.e., $C_L = 0$. In this case, one simply has to consider the upper half-plane defined by the streamline that impacts on the airfoil, since the other half has a reflected flow (see, e.g., Ref. 11 for the treatment of the compressible flow around a circular obstacle). It is obvious that the same cannot be done for other nonsymmetric airfoils, or, if one would like to design a symmetric airfoil at a nonzero incidence.

As will be seen, using a different idea, the method presented in this article extends the classical hodograph theory removing the failure produced by any kind of overlapping (without hypothesis of symmetry) R_V; in this way, it provides a complete generalization of the hodograph method for the problem of inverse airfoil design.

Ideal Fluid Dynamics Equations

The complex velocities of the motion of an ideal flow in a region R_Z can be defined in terms of the complex potential, as follows:

$$u - iv = qe^{-i\theta} = V = F(Z) = \frac{dW}{dZ} \tag{7}$$

one finds from this that $\nabla^2\psi = 0$, which coincides with Eq. (3) for $M = 0$.

A complex z plane that has an appropriate circular obstacle of radius R centered at the origin is defined. Then if the analytic function f

$$Z = f(z) \tag{8}$$

maps the region R_z exterior to the circular obstacle one-to-one and onto the region R_Z, it follows that there exists an analytic function G_V,

$$V = G_V(z) \tag{9}$$

which maps the region R_z of the z plane onto the region R_V in the hodograph. From the correspondence between Z and z it turns out that the circle that defines the circular obstacle will be mapped by G_V onto the velocity–contour.

Now, a summary of some results of Ref. 9 is given. These results are independent of the shape of the input VC. The forward stagnation or impact point S and the trailing edge T correspond to two other stagnation points z_S and z_T on the circular obstacle ($z = Re^{i\phi}$) in the z plane (see Fig. 6). From the flow equation around a circular obstacle of R, it turns out that these points, Γ, α, and q_0 satisfy:

$$z_S = Re^{i(\pi - b)} \tag{10}$$

$$z_T = Re^{i(b+2\alpha)} \tag{11}$$

$$2i \sin(b + \alpha) = -\frac{\Gamma}{2\pi i} \cdot \frac{1}{Rq_0} \tag{12}$$

From the equivalence of the planes far away from the airfoil and the circular obstacle, respectively, one gets:

$$V_0 = V_\infty \tag{13}$$

$$\alpha = \theta_\infty \tag{14}$$

For the particular cases of S of complex velocity $V_S = 0$ and for T of complex velocity $V_T = q_T e^{-i\theta_T}$, Eq. (9) gives

$$G_V(z_S) = 0 \tag{15}$$

$$G_V(z_T) = q_T e^{-i\theta_T} \tag{16}$$

The closure-compatibility at infinity condition is

$$2iRq_0 \sin(b + \alpha) = \left[\frac{dG_V(z)}{dz} \cdot z^2\right]_{z\to\infty} \tag{17}$$

The determination of the airfoil is reduced to a simple real integration of a complex integrand

$$Z(\phi_f) = -2q_0R \int_{\phi_0}^{\phi_f} \frac{1}{G_V(z)} [\sin(\phi - \alpha) - \sin(b + \alpha)]\, d\phi \tag{18}$$

The transformation G_V fixes a value for R, which can be chosen to be 1. It follows from Eqs. (10–14) and (18) that if the correct values of $V_\infty = q_\infty e^{-i\theta_\infty}$ and b, and the function $G_V(z)$ are found, the airfoil can be easily designed.

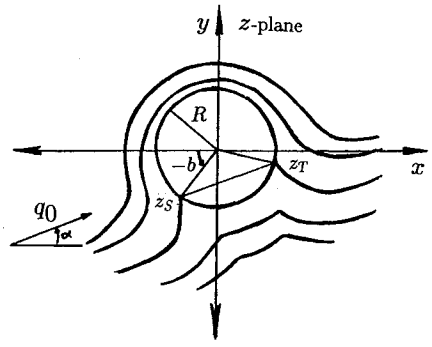

Fig. 6 Flow around a circular obstacle.

The equations of this section can be deduced without difficulty, so where do the previously discussed problems for overlapping R_V appear? As will be seen, they appear when one tries to find the explicit expression for $V = G_V(z)$. This is not surprising, since by definition G_V maps R_z onto R_V, and then it contains the information about the topology or shape of the region R_V. The velocity–contour affects G_V in the following ways:

1) If the VC is a simple (non-self-intersecting) contour, the function G_V is one-to-one. This follows from Eqs. (8) and (9) and from the one-to-one correspondence between the points of R_Z and R_V for non-self-intersecting VCs.

2) If the VC self-intersects, then G_V is not one-to-one. This follows from the relation between R_z and R_Z and from the fact that, in this case, the correspondence between R_Z and R_V is many-to-one.

Fast Method of Explicit One-to-One Mapping

A fast method to find the explicit analytic function that maps a circular contour into any given non-self-intersecting closed contour will be briefly described. It was used in Ref. 9 to find the G_V for all of the VCs that are non-self-intersecting closed curves.

Consider a $C_{\xi 0}$, which defines a simple (nonoverlapping) domain $R_{\xi 0}$ in a ξ_0 plane. Let $\xi_{0\infty}$ be an arbitrary point inside $R_{\xi 0}$, and ξ_{0S} a point of the contour $C_{\xi 0}$. It is possible to deduce that there exists a unique analytic function

$$G_0(z, b, \xi_{0\infty}) = \xi_0 \tag{19}$$

that maps the points z of the region R_z (outside the circular obstacle) one-to-one and onto the points ξ_0 of the region $R_{\xi 0}$, and such that it also maps the contour of the circular obstacle into the given simple closed-curve $C_{\xi 0}$ and the points $\xi_0 = \xi_{0\infty}$ and $\xi_0 = \xi_{0S}$ to the points $z = \infty$ and $z = e^{i(\pi - b)}$, respectively. Furthermore, it follows that G_0 has a well-defined inverse G_0^{-1}. By comparison with formulas of Ref. 9 (with $R_{\xi 0}$ as R_V, $\xi_{0\infty}$ as V_∞, ξ_{0S} as V_S, and $C_{\xi 0}$ as the non-self-intersecting VC), the explicit expression for the analytic function G_0 can be found in terms of the parameters b and $\xi_{0\infty}$ by the following expression:

$$G_4(e^{ib}z, \xi_{0\infty}) = G_0(z, b, \xi_{0\infty}) = \xi_0 \tag{20}$$

$$e^{-ib}G_4^{-1}(\xi_0, \xi_{0\infty}) = G_0^{-1}(\xi_0, b, \xi_{0\infty}) = z \tag{21}$$

where $G_4 = G_1 \cdot G_2 \cdot G_3$: (here and in the following, the symbol $\cdot$ between functions denotes composition, i.e., $f \cdot g(\xi) = f[g(\xi)]$). G_1 can be determined in terms of its inverse G_1^{-1}. G_1^{-1} is a sequence of very simple explicit analytic functions defined in Ref. 9 that transforms in a very fast way the given (arbitrary) $C_{\xi 0}$ (it can have corners) into a smooth quasicircular contour, at the same time it maps the region $R_{\xi 0}$ onto the in-

terior of the quasicircular contour and the point $\xi_{0\infty}$ into the origin. Finally, G_3 and G_2 are simply

$$G_3(w) = 1/w \tag{22}$$

$$G_2(w) = w \exp\left[\sum_{j=0}^{N} (A_j + iB_j)w^j\right] \tag{23}$$

where the coefficients A_j and B_j are determined using fast Fourier transform so that G_2 maps the interior of the circular disc onto the quasicircular contour.

As a consequence, for any non-self-intersecting $C_{\xi 0}$, one has a well-defined explicit one-to-one transformation $\xi_0 = G_0(z, b, \xi_{0\infty})$, which maps the region R_z onto $R_{\xi 0}$. Furthermore, the inverse G_0^{-1} exists and is a well-defined mapping.

If the VC self-intersects then this cannot be taken as the contour $C_{\xi 0}$, and then it is impossible to find the map from R_z onto R_V with the previous method. The problem is that this kind of VC cannot be continuously deformed into the circle. This continuous deformation would be performed by the inverse function of G_V, but G_V^{-1} does not exist because G_V is many-to-one.

Theoretical Development for Removing the Failure Caused by Overlapping Regions R_V

It is very important to note that according to the relation

$$\int \frac{1}{V}\frac{dW}{dz}\,dz = Z = \int \frac{1}{V}\frac{dW}{dV}\,dV \tag{24}$$

deduced in Eq. (5), the obstruction to finding W in the overlapped region R_V (as in the classic compressible hodograph method) is equivalent to the failure in finding the function $V = G_V(z)$.

The key to solving this problem is to consider R_V as a part of a structure that the mathematicians know as a Riemann surface. Two Riemann surfaces can be put into one-to-one correspondence when they are topologically equivalent. It turns out that R_V belongs to a two-sheeted Riemann surface, and the other region R_z belongs to a Riemann surface of one sheet. The correspondence is established by means of the definition of an analytic function h_j for each sheet j of each Riemann surface. These h_j are pasted with the following h_{j+1} at the branch cuts and all of them coincide at the branch points. Furthermore, the h_j turn out to be exactly the roots that define the Riemann inverse G_V^{-1} of an analytic function G_V called the generating function of the Riemann surface. The Riemann inverse G_V^{-1} should be at least two-valued so that the action of at least two root functions h_j spreads the domain defined by the zone of overlapping into two subregions.

The first step of the solution comes from the following fact. For any $C_{\xi 0}$ that defines a simply connected region $R_{\xi 0}$ in a ξ_0 plane, one can find an analytic function G_0 (constructively with the fast method of explicit one-to-one mapping) which defines a one-to-one correspondence between $R_{\xi 0}$ and R_z, then one has

$$\xi_0 = G_0(z) \quad \text{and} \quad z = G_0^{-1}(\xi_0) \tag{25}$$

where the inverse G_0^{-1} is well defined in the classical sense. Since the composition of two analytic functions is also an analytic function, composing G_0^{-1} and G_V in Eq. (9) one has

$$V = G_V[G_0^{-1}(\xi_0)] = G_L(\xi_0) \tag{26}$$

or

$$G_L \equiv G_V \cdot G_0^{-1} \quad \text{and} \quad G_V \equiv G_L \cdot G_0 \tag{27}$$

[observe that in Eqs. (26) and (27), the inverse of G_V has not been used because it is not defined in the classical sense]. It follows from its definition that G_L is not one-to-one and that it maps the simple closed contour $C_{\xi 0}$ of arbitrary shape onto the VC. The considerations on G_V and their roots are equally applicable to G_L. It follows from the second equality of Eq. (27) that if one finds explicitly G_L and determines $C_{\xi 0}$, one can determine G_0 and find, by composition, the analytic function G_V.

As a consequence the problem has been reduced to a simpler one. Now basically, one has to find an arbitrary analytic generating function G_L, such that its Riemann inverse G_L^{-1} maps the self-intersecting contour (VC) into an arbitrary simple (non-self-intersecting and without loops) closed-curve $C_{\xi 0}$.

Two effective methods (with their respective codes) using the previous theory have been developed. The first method is supported by physical reasons. It is basically a fit method, and it is suitable mainly for velocity–contours with loops. The second is mathematical, simple and general.

Method 1 for the Treatment of VCs with Loop

The method can be summarized as follows. Fit the input VC (with a loop) with another auxiliary VC (with a loop), which has an explicit $G_V \equiv G_{\text{aux}}$ generated by a known airfoil. Since the Riemann inverse of this G_{aux} maps by definition the auxiliary VC with loop into a contour without loops (the circle), one can expect that, if the fit is good, the application of the Riemann inverse G_{aux}^{-1} of G_{aux} on the input VC will map it into an arbitrary auxiliary contour, but without loops. According to what was stressed in the last section, this is exactly what one was looking for. The arbitrary auxiliary contour and G_{aux} play the role of $C_{\xi 0}$ and G_L, respectively.

Now, one has to find airfoils of known shape, from which one can generate explicit expressions of auxiliary G_V. Suppose that one knows an analytic explicit function f_L,

$$Z = f_L(z) \tag{28}$$

which defines the coordinates Z of an airfoil for values of z along the boundary of a circular obstacle, and such f_L tends to the identity function when $z \to \infty$. It follows that

$$V = G_{\text{aux}}(z) = \left[q_{0L}e^{-i\alpha_L} - q_{0L}e^{i\alpha_L}\frac{1}{z^2} - q_{0L}2i\sin(\phi_t - \alpha_L)\frac{1}{z}\right] \times \frac{1}{\left[\dfrac{df_L(z)}{dz}\right]} \tag{29}$$

determines the complex velocity of the airfoil for any velocity of incidence $q_{0L}e^{-i\alpha_L}$, and where ϕ_t is the angle on the circular obstacle that corresponds to the trailing edge of the airfoil. By comparison with Eq. (9), it follows that Eq. (29) defines a general explicit auxiliary $G_V \equiv G_{\text{aux}}$. If the airfoil associated to f_L is capable to generate VCs with loops, then one deduces that the general function G_L for removing loops defined in Eq. (27) is

$$G_L = G_{\text{aux}} \cdot G_3 \tag{30}$$

with G_3 defined in Eq. (22), and the Riemann inverse G_L^{-1} is finally expressed in terms of the Riemann inverse G_{aux}^{-1} of G_{aux}:

$$G_L^{-1} = G_3^{-1} \cdot G_{\text{aux}}^{-1} = G_3 \cdot G_{\text{aux}}^{-1} \tag{31}$$

The next step consists of finding some f_L. The author proposes the following airfoil generating transformation (JLT):

$$Z = w + \frac{H^2(\beta)}{w^\beta} \tag{32}$$

where β is a real constant that satisfies $1 \leq \beta \leq \infty$, and H is another constant that depends on β and on the real point w_t:

$$H(\beta) = \sqrt{(w_t^{\beta+1}/\beta)} \tag{33}$$

w_t corresponds to the trailing edge of the airfoil and is a point on the circle of R_L centered at the point c

$$c = -c_r + ic_i \tag{34}$$

where, without loss of generality, c_r and c_i are positives. The JLT reduces to the identity for $\beta = \infty$ and to the classical Joukowski transformation for $\beta = 1$. If one defines the translation

$$z = w - c \tag{35}$$

the circle will be centered at the origin. In particular, for the points corresponding to the trailing edge, one has

$$z_t = w_t - c = w_t + c_r - ic_i \tag{36}$$

writing $z_t = R_L e^{i\phi_t}$ and equating real and imaginary parts in Eq. (36) one obtains

$$\arcsin(c_i/R_L) = -\phi_t \tag{37}$$

$$w_t = \sqrt{R_L^2 - c_i^2} - c_r \tag{38}$$

This implies that one can choose arbitrarily the parameter β, the radius $R_L = 1$, and the position of the center c of the circular obstacle; these conditions fix the value of w_t and $H(\beta)$. Writing the transformation as a function of z by means of Eq. (35) one has

$$Z = f_L(z) = z + c + [H^2(\beta)/(z + c)^\beta] \tag{39}$$

and replacing this into Eq. (29), one gets

$$V = G_{\text{aux}}(z) = [q_{0L}e^{-i\alpha_L} - q_{0L}e^{i\alpha_L}(1/z^2) - q_{0L}2i \times \sin(\phi_t - \alpha_L)(1/z)] \frac{1}{\{1 - [w_t^{\beta+1}/(z + c)^{\beta+1}]\}} \tag{40}$$

Now, one has to determine the Riemann inverse G_{aux}^{-1}. To do this one rewrites Eq. (40) as

$$0 = [q_{0L}e^{-i\alpha_L}z^2 - q_{0L}e^{i\alpha_L} - q_{0L}2i \sin(\phi_t - \alpha_L)z](z + c)^{\beta+1} - [(z + c)^{\beta+1} - w_t^{\beta+1}]z^2V \tag{41}$$

Then, for given values of the fit parameters (q_{0L}, α_L, c, β) one has to find the values of z (the roots), which satisfy Eq. (41) for each value of V. The solution is complicated unless $\beta + 1$ is an integer. This implies that $\beta = (1, 2, 3, \ldots)$, then for integer values of β, the right-hand side (RHS) of Eq. (41) reduces to a polynomial of degree $\beta + 3$ in z. The problem now consists of the determination of the $\beta + 3$ roots $[z_{1V}, z_{2V}, \ldots, z_{(\beta+3)V}]$ as a function of V. This determination can be done numerically with a program of determination of roots for complex polynomials, with Laguerre's method.[12] The selection of the correct root among the $\beta + 3$ roots can be deduced from the fact that, for complex velocities V on the VC, the selected roots have to form a closed contour without loops routed in the appropriate direction. But, what is the specific value of β that one should take? Fortunately, the answer is that one can take the value $\beta = 1$. This is the best answer that one can expect: if $\beta = 1$, the degree of the polynomial is minimal so that one has to find only the minimum number $\beta + 3 = 4$ of roots, but the most important fact is that for $\beta = 1$, G_{aux}^{-1} preserves the smoothing of the contours.

Then, taking $\beta = 1$, the RHS of Eq. (41) reduces to a polynomial of degree 4 in z:

$$0 = [q_{0L}e^{-i\alpha_L}z^2 - q_{0L}e^{i\alpha_L} - q_{0L}2i \sin(\phi_t - \alpha_L)z] \times (z + c)^2 - [(z + c)^2 - w_t^2]z^2V \tag{42}$$

An appropriate factorization reduces the degree in one and finally one has

$$\left(\frac{V}{q_{0L}e^{-i\alpha_L}} - 1\right) z^3 + \left[\frac{(c + w_t)V}{q_{0L}e^{-i\alpha_L}} - 2c + e^{i\phi_s}\right] z^2 + (-c^2 + 2ce^{i\phi_s})z + e^{i\phi_s}c^2 = 0 \tag{43}$$

where

$$\phi_s = \pi + 2\alpha - \phi_t \tag{44}$$

Then, one simply has to find for each V along the VC the three roots of Eq. (43), the roots will define three contours and one of them will be without a loop; then applying G_3 on this selected contour [according to Eq. (30) and the definition of G_L], the auxiliary contour $C_{\xi 0}$ without loops and its corresponding region $R_{\xi 0}$ will be determined. With the use of the fast method of explicit one-to-one mapping, one can find afterwards, the complete mapping G_V, that according to Eqs. (27) and (30) will be given by

$$G_V = G_L \cdot G_0 = G_{\text{aux}} \cdot G_3 \cdot G_0 \tag{45}$$

Furthermore from Eqs. (20) and (21):

$$G_V^{-1} = G_0^{-1} \cdot G_L^{-1} = e^{-ib}G_4^{-1} \cdot G_L^{-1} \tag{46}$$

Denoting by η_{self} the set of fitting parameters (q_{0L}, α_L, c), which defines G_L, remembering that G_0 depends on b and $\xi_{0\infty}$ (or equivalently on V_∞) one can write:

$$V = G_V(z, \eta_{\text{self}}, b, V_\infty) \tag{47}$$

$$z = G_V^{-1}(V, \eta_{\text{self}}, b, V_\infty) \tag{48}$$

Method 2 for the Treatment of Any Self-Intersecting VC

The method originates in the study of polynomial functions

$$0 = a_0(V) + a_1(V)\xi_0 + a_2(V)\xi_0^2 + \cdots + a_N(V)\xi_0^N \tag{49}$$

which is the most general expression for removing the self-intersection of the VC and can be viewed as an implicit form of Eq. (26): $V = G_L(\xi_0)$. Observe that Eq. (43) is a particular case of Eq. (49) with z as ξ_0. Looking for the most simple (but effective) solution and taking into account that here one is working with a two-sheet Riemann surface, one can take $N = 2$ in Eq. (49)

$$0 = a_0(V) + a_1(V)\xi_0 + a_2(V)\xi_0^2 \tag{50}$$

Then for any value of V, and since there is no loss of generality when using Eq. (50), it follows that:

$$\xi_0 = G_L^{-1}(V) = \frac{-a_1(V) \pm \sqrt{a_1^2(V) - 4a_0(V)a_2(V)}}{2a_2(V)} \tag{51}$$

Finally, the most simple function for removing self-intersection of the VC is

$$\xi_0 = G_L^{-1}(V) = \frac{-a_1 \pm \sqrt{a_1^2 - 4(a_0 - V)a_2}}{2a_2} \tag{52}$$

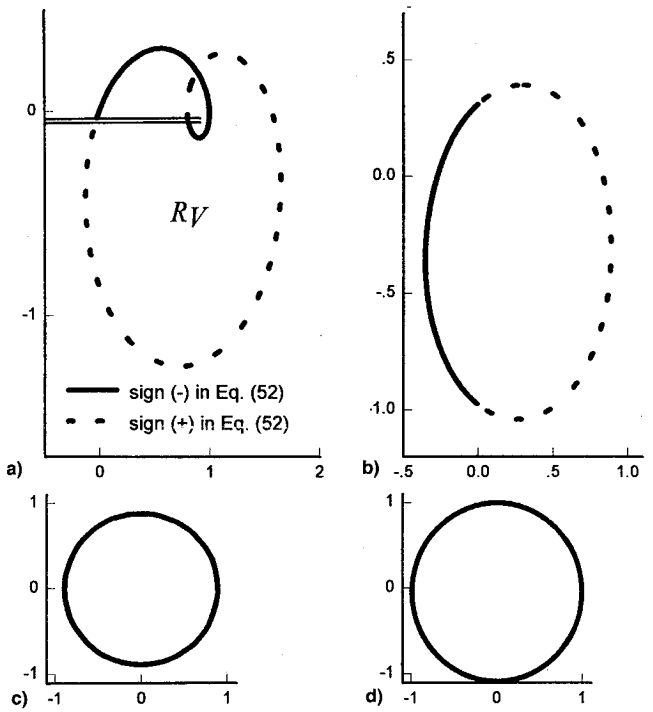

Fig. 7 Successive mapping of a self-intersecting velocity–contour (generated by a Joukowski airfoil) into the circular contour: a) input velocity–contour; b) setting a one-to-one connection, domain inside of a non-self-intersecting contour; c) domain inside of a quasicircular contour; and d) domain outside of a unitary circular contour.

where now a_0, a_1, a_2 are constants such that for a VC of the case 1 satisfy

$$a_1^2 = 4a_2(a_0 - V_{\text{loop}}) \tag{53}$$

where V_{loop} is an arbitrary point of the interior of the loop zone, and such that for a velocity–contour of case 2, they satisfy

$$a_1^2 = 4a_2(a_0 - V_{\text{hole}}) \tag{54}$$

together with the condition that the branch cut has to pass through the zone of overlapping which imposes another constraint on one of the a_i. V_{hole} is an arbitrary point of the interior of the hole inside R_V.

Calculating the two values of ξ_0 for all of the values V along the velocity–contour, one obtains two closed contours. The resulting contours are non-self-intersecting, and so any one of both contours can be taken as the contour $C_{\xi 0}$. One part of the contour is formed by the ξ_0 obtained with the positive sign of Eq. (52), and the other part with the negative sign. The change of sign comes exactly when the VC passes through the branch cut of the square root of Eq. (52). This is shown in Fig. 7a where one can see an input velocity–contour with a loop (case 1). There, the two-parallel lines that begin in the interior of the loop (zone of overlapping) at the point V_{loop} represent the square root's branch cut. The points of the dashed line in the VC correspond to the positive sign of the square root and the points of the continuous line in the VC to the negative sign. The contour selected as the $C_{\xi 0}$ is shown in Fig. 7b. The points corresponding to the positive and negative sign of the square root of Eq. (52) are still shown as a dashed and continuous line, respectively. Similar steps can be followed for a VC of the type of case 2 as the one shown in Fig. 7b; in this case the origin of the branch cut corresponds to the point V_{hole}. Then it follows that one can express G_V and its Riemann inverse as in Eqs. (27) and (46), but with G_L^{-1} given now by Eq. (52), and with

$$V = G_L(\xi_0) = a_0 + a_1\xi_0 + a_2\xi_0^2 \tag{55}$$

Denoting now by η_{self} the set of parameters $[a_1, a_2, V_{\text{loop}}$ (or $V_{\text{hole}})]$, one can write equations similar to Eqs. (47) and (48), and so one also has

$$V = G_V(z, \eta_{\text{self}}, b, V_\infty) \quad \text{and} \quad z = G_V^{-1}(V, \eta_{\text{self}}, b, V_\infty) \tag{56}$$

By extending this method one can treat the case of a VC with more than one loop.

Determination of the Unknown Parameters

Following analogous steps to the ones followed in Ref. 9 and using Eqs. (10–17), (20), (21), (27), and (46), one deduces that

$$2iRq_\infty \sin[B_b(V_\infty) + \theta_\infty]e^{iB_b(V_\infty)} = \left[\frac{dG(\xi, \eta_{\text{self}}, V_\infty)}{d\xi} \cdot \xi^2\right]_{\xi\to\infty} \tag{57}$$

with

$$b = B_b(V_\infty) = \tfrac{1}{2}\arg[-R^{-2}G^{-1}(V_T, \eta_{\text{self}}, V_\infty)\overline{G^{-1}(0, \eta_{\text{self}}, V_\infty)}] - \theta_\infty \tag{58}$$

where the overbar $\overline{w}$ means complex conjugate of w

$$G = G_L \cdot G_4 \quad \text{and} \quad G^{-1} = G_4^{-1} \cdot G_L^{-1} \tag{59}$$

and the dependence of G on η_{self} and V_∞ has been made explicit. Then, one can determine V_∞ by means of Eq. (57), then b by means of Eq. (58), and the rest of the coefficients by means of Eqs. (10–17). Finally, the airfoil can be determined by

$$Z(\phi_f) = -2Rq_\infty \int_{\phi_0}^{\phi_f} \frac{1}{G_V(z, \eta_{\text{self}}, b, V_\infty)} [\sin(\phi - \theta_\infty) - \sin(b + \theta_\infty)]\, d\phi \tag{60}$$

Important Results

A comparison shows that the final Eqs. (57) and (58) reduce to the same final equations of Ref. 9 if G_L is taken as the identity, i.e., one only has to set $G_L \equiv I$ when the velocity–contour is a non-self-intersecting contour. Keeping this in mind, the present inverse method becomes general, and can then be used to design airfoils for any input VC (with or without self-intersection or loops).

It is important to remark that for a self-intersecting VC, a new set of parameters expressed as η_{self} has been added to the pre-existent (b and V_∞). What does this mean? One may think that for a given self-intersecting VC the values defined by η_{self} are fixed. If this were true nothing would have changed with respect to the case of non-self-intersecting VCs. On the contrary, the parameters defined by η_{self} can vary almost freely, for example, in method 2 the point V_{loop} can be any of the interior points of the zone of overlapping. Furthermore, there are no fluid dynamics equations imposing restrictions on η_{self}.

Then, for each set η_{self}, one can obtain a complex number V_∞ [from Eq. (57)] and as a consequence an airfoil [from Eq. (60)]. This, together with the existence of an infinite number of η_{self} values, permits the deduction of the following: In contrast to the case of a non-self-intersecting VC for which a unique airfoil and its corresponding V_∞ exist; in the case 1 of a self-intersecting VC with loop, there not only exists one airfoil, but an infinite number of different airfoils with their respective design condition V_∞, which on their surface generate

exactly the velocities (speed and direction) prescribed in the velocity–contour.

The same result is not valid for the cases of an R_V with a hole (i.e., for self-intersecting VCs belonging to case 2, as the one shown in Fig. 5b). In this case, independently of the values given to the set of paramenters η_{self}, one always obtains the same airfoil, and then this case is similar to the case of non-self-intersecting contours.

From a mathematical point of view, a deeper analysis shows the causes for these surprising results: A calculation of the Jacobian J [Eq. (6)] gives the following:

1) For a VC belonging to case 1: $J \neq 0$ everywhere except for the point $u - iv = V_{loop}$ (where always $J = 0$), which corresponds to a point inside the flow region R_Z.

2) For a VC belonging to case 2: $J \neq 0$ everywhere except for the point $u - iv = V_{hole}$ (where always $J = 0$), which corresponds to a point out of the region R_Z. It is apparent that the vanishing of the Jacobian in a point inside the region R_Z gives a new degree (or parameter) of freedom for the design. Results 1 and 2 are consistent with the compressible hodograph theory, where it is established that for subsonic flow the Jacobian can vanish only at isolated points.

From a physical viewpoint, the result that there may be many airfoils that generate the same velocity–contour can be more easily understood if one compares how the method of this article and the nonhodograph inverse methods work. In the latter cases the distribution of velocities $q = q(s)$ is given. This fixes uniquely the variation of speed Δq in a specified Δs along each point s of the airfoil's surface and the circulation Γ generated by the airfoil. By unicity of the harmonic conjugates, the distribution specified $q = q(s)$ along the airfoil's surface, is equivalent to a unique distribution of complex velocities $V = V(\phi)$ specified along the circular obstacle's surface into which the airfoil can be mapped, from this one deduces that a unique airfoil may exist. On the other hand, for the case of the hodograph method presented here, the airfoils are designed by prescribing the shape of the VC and the point V_T that corresponds to the trailing-edge velocity of the airfoil. The VC does not contain information on the arc length s of the airfoil. Herein lies the point: the method presented in this article is able to find what is the appropriate arc length Δs that corresponds to each variation of speed Δq specified at the VC. In particular, the Γ of the airfoil and the V_∞ (direction and speed) are not imposed. Their values are found automatically by the method in such a way that the physical constraints be satisfied. When the VC does not have loops a unique appropriate Δs exists for each variation of speed Δq, i.e., a unique distribution $q = q(s)$ exists. However, when the VC has loops, the added degree of freedom provided by η_{self} permits other appropriate Δs for the same Δq. This will correspond to other physically meaningful airfoils. The method presented here does not work with a unique complex velocity distribution $V = V(\phi)$; it takes into account all of the complex velocity distributions of the type $V = V[D(\phi)]$, where D stands for all of the analytic one-to-one diffeomorphisms of the circle in the circle.

In the following, two examples will illustrate and test the method. The tests will be as follows: choose any airfoil of known shape and for any freestream velocity $V_l = q_l e^{-i\theta_l}$ calculate the corresponding VC by means of an arbitrary direct method (e.g., a panel method), if a self-intersecting VC results, take it as the input of the present method. Will the method then be able to find a solution for this meaningful VC? Will it actually verify the existence of an infinite number of airfoils with exactly the same VC? Will all of these airfoils be really different? If one is able to obtain a freestream velocity of design $V_\infty = q_\infty e^{-i\theta_\infty}$, which is practically equal to the velocity $V_l = q_l e^{-i\theta_l}$, will the designed airfoil be exactly equal to the known airfoil from which the input VC was taken? The answer to all of these questions, as will be seen, is positive.

Example 1: Redesign of the NACA 0012 and Design of Its Similar Airfoils

The NACA 0012 is a well-known symmetrical airfoil, and without leading-edge corrections its coordinates (X, Y) with $0 \leq X \leq 1.00893$ are defined by the following equation:

$$Y = (t/0.2)(0.2969\sqrt{X} - 0.126X - 0.3516X^2 + 0.2843X^3 - 0.1015X^4) \quad (61)$$

where $t = 0.12$ is the relative thickness (see Ref. 13). The trailing-edge angle ε_T is equal to 16.15 deg. Using a panel method, the velocity–contour corresponding to the freestream velocity $V_l = q_l e^{-i\theta_l}$, with $q_l = 1$ and $\theta_l = 4$ deg can be determined. This VC is shown in Fig. 4 and will be used as input in the computational code of the method. The complex velocity V_T of the trailing edge turns out to be $V_T = 0 + i0$, since the NACA 0012 has a trailing-edge angle $\neq 0$.

For this example the method 1 for the treatment of VCs with loop will be used. One proceeds to give values to the fit parameters (q_{0L}, α_L, $c = -c_r + ic_i$), which defines η_{self}. The values of c_r are usually taken between $0.25-0.08R$, and the ones of c_i between c_r and 0. Here, the values of c_r and c_i were maintained fixed at 0.16 and 0., respectively. First, the values $q_{0L} = 1$ and $\alpha_L = 2$ deg, were chosen, and the code proceeds to the determination of the airfoil as follows: Eq. (43) is solved to find three roots for each V of the input VC, the results are shown in Fig. 8b, where the three sets of roots (corresponding to each square point on the VC of Fig. 8a) have been graphed by square points. Then the roots that contribute to the formation of the auxiliary non-self-intersecting (without loop) contour are selected; the resulting non-self-intersecting contour is shown in Fig. 8b with a continuous line. Once this auxiliary contour is determined, the method finds (by the application of G_3) the contour $C_{\xi 0}$ (shown in Fig. 8c) and the functions G_L and G_L^{-1} according to Eqs. (40) and (43). Having defined the new contour $C_{\xi 0}$, the code determines the transformation of this contour into the circular contour as shown in Fig. 8d (tak-

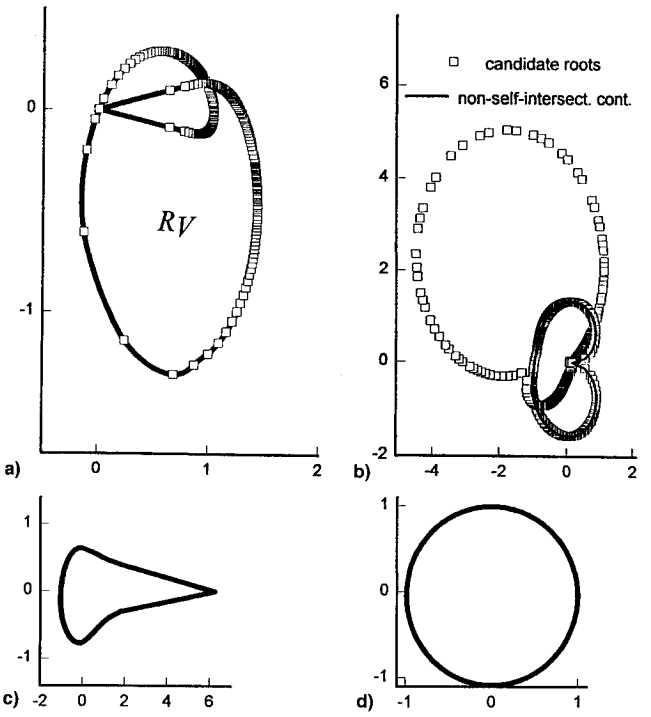

Fig. 8 Successive mapping of a self-intersecting velocity–contour (generated by the NACA 0012 airfoil) into the circular contour: a) input velocity–contour; b) setting a one-to-one connection, domain outside of the candidate contour; c) domain inside of a simple contour with a corner; and d) domain outside of a unitary circular contour.

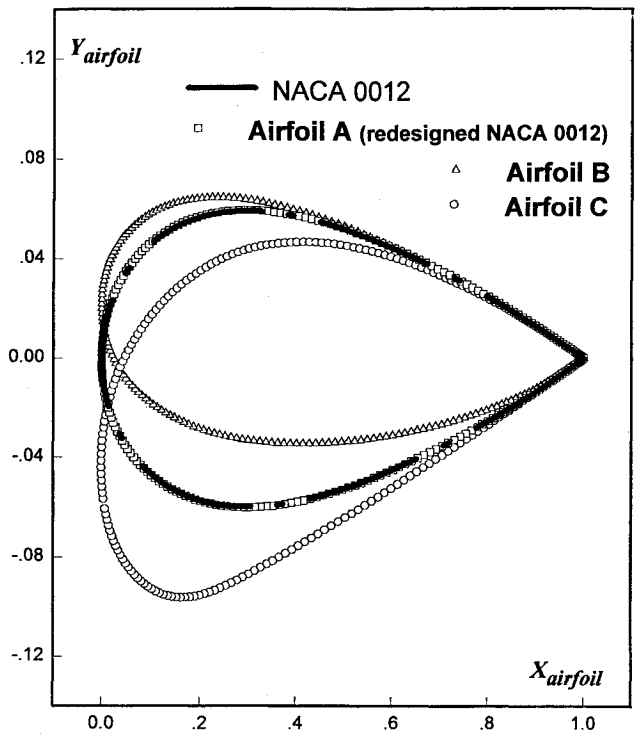

Fig. 9 NACA 0012 and three designed airfoils with the same velocity–contour.

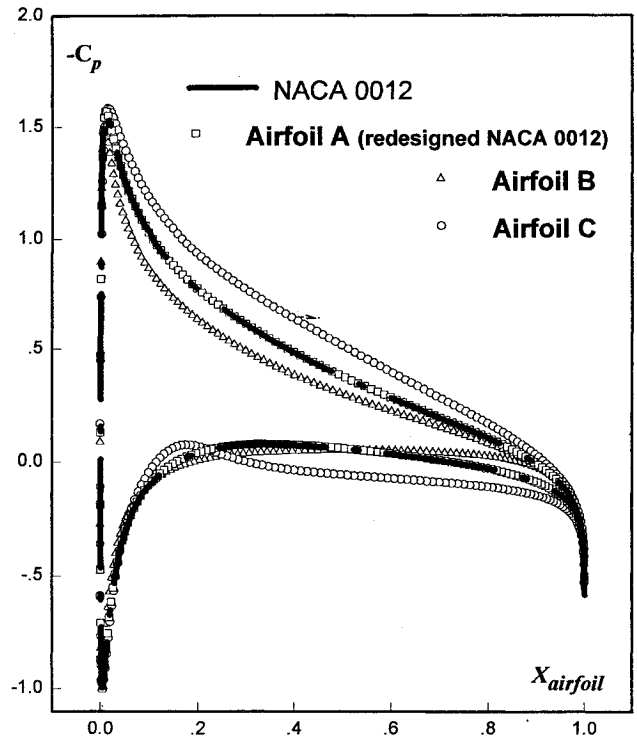

Fig. 10 Pressure distributions of the A, B, and C airfoils at their design conditions.

ing into account that, as a consequence of the fact that the trailing-edge angle is $\neq 0$, there is a corner, as can be seen in Fig. 8c, of angle 16.15 deg that has to be removed), and as a consequence finds G_0 and G_4. With the functions G_0, G_4, and G_L, the functions G_V^{-1}, G_V, and G are determined by means of Eqs. (45), (46), and (59). Then, it finds the value V_∞ that satisfies Eq. (57) and determines all of the unknown coefficients (b, q_0, $R = 1$, α, ϕ_S, Γ, ϕ_T) by means of Eqs. (58) and (10–17). Finally, the airfoil is determined by means of Eq. (60).

For the given values of $q_{0L} = 1$ and $\alpha_L = 2$ deg, the values $q_\infty = 1.01198$ and $\theta_\infty = 2.42226$ deg for $V_\infty = q_\infty e^{-i\theta_\infty}$, which satisfy Eq. (57) were obtained. And the resulting airfoil is the airfoil B shown in Fig. 9. Starting again the program with new values $q_{0L} = 1$ and $\alpha_L = 6.6$ deg, the values $q_\infty = 0.99936$ and $\theta_\infty = 6.53501$ deg for $V_\infty = q_\infty e^{-i\theta_\infty}$ that satisfy Eq. (57) were obtained, and the resulting airfoil is airfoil C shown in Fig. 9. For new values of q_{0L} and α_L, new and different airfoils were obtained, in particular for $q_{0L} = 0.9915$ and $\alpha_L = 3.67$ deg, the values $q_\infty = 0.99969$ and $\theta_\infty = 4.00796$ deg for $V_\infty = q_\infty e^{-i\theta_\infty}$ and airfoil A were obtained. These latter values of q_∞ and θ_∞ differ with respect to $q_l = 1$ and $\theta_l = 4$ deg only in a percentage of 0.03% in the speed and in 8 thousandths of degree in the incidence. Then, remembering that for these values of q_l and θ_l the NACA 0012 airfoil generates the input VC, if all in the theory is right, the designed airfoil, airfoil A, should be practically equal to the NACA 0012 airfoil, and as can be appreciated in Fig. 9, it is indeed. Then, airfoil A can be considered as the redesigned NACA 0012 airfoil. An analysis with a panel method has confirmed that airfoils A, B, and C have the same VC as the NACA 0012 airfoil. Figure 10 shows the distribution of the pressure coefficient $C_p = 1 - (q/q_\infty)^2$ for these airfoils.

Example 2: Redesign of a Joukowski Airfoil and Design of Its Similar Airfoils

Here, the VC of a nonsymmetrical Joukowski airfoil was taken as input. The Joukowski airfoil can be determined from Eqs. (37–39) with $\beta = 1$, $R_L = 1$, $c = -c_r + ic_i = -0.15 + i0.075$, $H(1) = w_t$. Then, the VC was determined for the free-stream complex velocity $V_l = q_l e^{-i\theta_\infty}$, with $q_l = 1$ and $\theta_l = 5$ deg. The complex velocity V_T of the trailing edge turns out to be $V_T = (0.82664, 0.12505)$. The VC is shown in Fig. 3. For this example, the code with method 2 for the treatment of self-intersecting VCs was used.

One proceeds to give values to the parameters a_0, a_1, a_2, and V_{loop}, which define η_{self}. The parameters a_1, a_2, and V_{loop} can be chosen freely with the sole restriction that V_{loop} be one of the (infinitely many) points of the interior of the loop zone. The remaining coefficient a_0 has only to satisfy Eq. (53). For our examples the values were fixed as follows: $a_1 = 0 + i0$, $a_2 = 1 + i0$, and $a_0 = V_{\text{loop}}$. For the first example, the value for V_{loop} was $V_{\text{loop}} = 0.9 + i0$. With the parameters fixed, the program begins calculating the appropriate root ξ_0 for each V along the input VC, i.e., uses the sign (+) in Eq. (52) from the first point of the VC that meets the branch cut until it finds a new point that meets the branch cut (dashed line in the VC shown in Fig. 7a), then it changes to the sign (−) until finishing the route (continuous line in the VC shown in Fig. 7a). Once this is done, the selected roots define $C_{\xi 0}$, i.e., a non-self-intersecting contour as the one shown in Fig. 7b. Then, the program proceeds to transform the $C_{\xi 0}$ into the circular obstacle as shown in Figs. 7c and 7d, this determines G_0 and G_4. With the functions G_0, G_4, and G_L [which are given by Eq. (55)], the functions G_V^{-1}, G_V, G are determined by means of Eqs. (27), (46), and (59). Then, Eq. (57) is solved to find the value of V_∞ and the code determines all of the unknown coefficients (b, q_0, $R = 1$, α, ϕ_S, Γ, ϕ_T) by means of Eqs. (58) and (10–17). Finally, the airfoil is determined by means of Eq. (60).

For the given value of $V_{\text{loop}} = 0.9 + i0$, the values $q_\infty = 0.95264$ and $\theta_\infty = 0.66877$ deg for $V_\infty = q_\infty e^{-i\theta_\infty}$, which satisfy Eq. (57), were obtained. And the resulting airfoil is the airfoil E shown in Fig. 11. Starting again the method with a new value $V_{\text{loop}} = 0.9 - i0.121$, the values $q_\infty = 1.02529$ and $\theta_\infty = 7.22671$ deg for $V_\infty = q_\infty e^{-i\theta_\infty}$, which satisfy Eq. (57), were obtained, and the resulting airfoil is airfoil F shown in Fig. 11. For new values of V_{loop} new and different airfoils were obtained, in particular for $V_{\text{loop}} = 0.91 - i0.079$, the values $q_\infty = 1.00096$ and $\theta_\infty = 4.99354$ deg for $V_\infty = q_\infty e^{-i\theta_\infty}$ and airfoil D were obtained. These latter values of q_∞ and θ_∞ differ with respect to $q_l = 1$ and $\theta_l = 5$ deg, only in a percentage of 0.004% in the speed and in less than 7 thousandths of degree in the incidence. Then, remem-

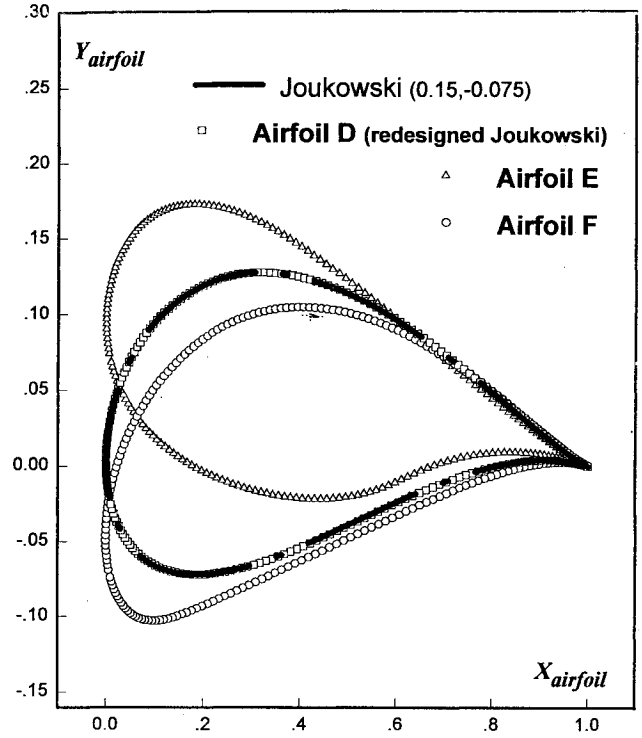

Fig. 11 Joukowski airfoil and three designed airfoils with the same velocity–contour.

bering that for these values of q_l and θ_l the Joukowski airfoil generates the input VC, the designed airfoil D should be practically equal to the Joukowski airfoil, and effectively it is, as it can be appreciated in Fig. 11. As a consequence the method has been capable of redesigning the Joukowski airfoil having as input its velocity–contour. Again, a verification with a panel method has confirmed that airfoils D, E, and F have the same VC.

Some final observations are as follows:

1) One should be careful with the examples given in Ref. 9 because it may be apparent that different airfoils can be obtained with a unique non-self-intersecting VC. This is not so since there it was necessary to modify the point V_T corresponding to the trailing-edge velocity to obtain new airfoils. It is obvious that this formally changes the velocity–contour, even if there is no apparent change in the shape of it.

2) The physical solutions found in the examples of this article prove the validity of the method developed here.

3) The method is exact. Furthermore, the airfoil is found at once: no successive modifications of a given airfoil are required.

4) In contrast to the nonhodograph methods, the values of q and θ can be specified simultaneously.

5) Since an arbitrary velocity distribution $q = q(s)$ or $q = q(\phi)$ does not neccessarily generate a physically meaningful airfoil, the methods[1–6] have to add to the prescribed ideal distribution some properly parametrized corrections, so that the parameters adjust the distribution to meet the physical constraints: gap at trailing edge or closure of the airfoil, continuity of the contour that defines the airfoil's boundary and compatibility at infinity. On the contrary, in the method developed here there is no need to modify or add corrections to the VC to find the airfoils, the parameters V_∞ and b (or Γ) that satisfy the constraints are naturally incorporated into the method.

Conclusions

The purpose of this article has been to present a mathematical development that provides an extension of the classical hodograph method. The extended theory removes the cases where the old theory fails. The failures occur when there is a many-to-one relation between the points of the physical plane and the space of velocity vectors. Then the mathematical theory (based on the theory of Riemann surfaces) has been applied to the case of inverse airfoil design. As a consequence the problem of inverse airfoil design for any self-intersecting velocity–contour has been successfully solved. The theory can be coupled with the previous work of Ref. 9, and so a unique computational code has been developed for the design of airfoils that satisfy all of the requirements imposed via any (self-intersecting or non-self-intersecting) input velocity–contour. Furthermore, a surprising result has been found: there is an infinite number of airfoils that generate exactly the same self-intersecting velocity–contour, contrary to the cases of simple velocity–contours for which there exists a unique airfoil. This surprising result shows that when the Jacobian J vanishes in the flow region, one gains a degree of freedom in comparison with the cases where $J \neq 0$ everywhere in the flow region. This implies an important consequence: in the design of airfoils that generate velocity–contours with loops, the designer can prescribe, together with the required velocity–contour corresponding to the airfoil's boundary, the desired speed q_∞ of the freestream (over a certain range). Finally, further investigation should be oriented to the study of the extension of the mathematical theory, developed here, to the case of transonic flows.

Acknowledgments

Thanks to C. Limache, G. Porta, G. Raggio, and J. Tamagno for their assistance and useful comments.

References

[1]Lighthill, M. J., "A New Method of Two-Dimensional Aerodynamic Design," British Aeronautical Research Council, R&M 2112, London, June 1945.

[2]Liebeck, R. H., "A Class of Airfoils Designed for High Lift in Incompressible Flow," *Journal of Aircraft*, Vol. 10, No. 10, 1973, pp. 610–617.

[3]Woods, L. C., "The Design of Two-Dimensional Aerofoils with Mixed Boundary Conditions," *Quarterly Journal of Applied Mathematics*, Vol. 13, No. 2, 1955, pp. 139–146.

[4]Volpe, G., "Inverse Airfoil Design: A Classical Approach Updated for Transonic Applications," *Applied Computational Aerodynamics*, edited by P. A. Henne, Vol. 125, Pt. 3, Progress in Astronautics and Aeronautics, AIAA, Washington, DC, 1990, pp. 191–220, Chap. 7.

[5]Jameson, A., "Computational Algorithms for Aerodynamic Analysis and Design," INRIA 25th Anniversary, Conf. on Computer Science and Control, France, Dec. 1992.

[6]Giles, M. B., and Drela, M., "Two-Dimensional Transonic Aerodynamic Design Method," *AIAA Journal*, Vol. 25, No. 9, 1987, pp. 1199–1206.

[7]Bauer, F., Garabedian, P., and Korn, D., "Supercritical Wing Sections," *Lecture Notes in Economics and Mathematical Systems*, Springer–Verlag, New York, 1972.

[8]Cohen, M. J., "High-Lift Airfoil Design from the Hodograph," *Journal of Aircraft*, Vol. 21, No. 10, 1984, pp. 760–766.

[9]Limache, A. C., "Inverse Method for Airfoil Design," *Journal of Aircraft*, Vol. 32, No. 5, 1995, pp. 1001–1011.

[10]Von Mises, R., Geiringer, H., and Ludford, G. S. S., *Mathematical Theory of Compressible Fluid Flow*, Academic, New York, 1959.

[11]Kuo, Y. H., and Sears, W. R., "Plane Subsonic and Transonic Potential Flow," *High Speed Aerodynamics and Jet Propulsion*, edited by W. R. Sears, Vol. VI, General Theory of High Speed Aerodynamics, Princeton Univ. Press, Pt. F, Sec. 8, Princeton, NJ, pp. 521–531.

[12]Press, W. H., Flannery, B. P., Teukolski, S. A., and Vetterling, W. T., "Numerical Recipes—The Art of Scientific Computing (Fortran Version)," *Root Finding and Nonlinear Sets of Equations. Section 9.5: Roots of Polynomial*, Cambridge Univ. Press, Cambridge, England, UK, 1989, pp. 259–269, Chap. 9.

[13]Abbott, I. H., and Von Doenhoff, A. E., "Theory of Wing Sections," *Families of Wing Sections. Section 6.4: NACA Four-Digit Wing Sections*, 2nd ed., Dover, New York, 1959, pp. 113, 114.